PCCP

Accepted Manuscript

Correlation among physical and electrochemical behaviour of nanostructured electrolytic manganese dioxide from leach liquor and synthetic for aqueous asymmetric capacitor

Manickam Minakshi Sundaram[1,*] Avijit Biswal[1,2], David Mitchell[3], Rob Jones[4] and Carlos Fernandez[5]

[1]*School of Engineering and Information Technology, Murdoch University, Murdoch, WA 6150, Australia*

[2]*CSIR-Institute of Minerals and Materials Technology, Bhubaneswar 751013, Odisha, India*

[3]*Electron Microscope Centre, Australian Institute for Innovative Materials, Innovation Campus, University of Wollongong, North Wollongong, NSW 2500, Australia*

[4]*Centre for Materials and Surface Science, La Trobe University, Bundoora, VIC 3086, Australia*

[5]*School of Pharmacy and Life Sciences, Robert Gordon University, Aberdeen AB10 7GJ, UK*

Abstract

An attempt has been made to correlate the differences in structural parameters, surface areas, morphology etc. with the electrochemical capacitive behaviour of the EMDs. The nanostructured electrolytic manganese dioxides (EMD) have been synthesized through electrodepositing MnO_2 from two different leach liquors and a synthetic analogue thereof. The structural and chemical state was determined using x-ray diffraction (XRD) and x-ray photoelectron spectroscopy (XPS) respectively. Multiplet structure determination led to estimates of the manganese valence states present in the EMD. The EMDs have been tested in an asymmetric capacitor which we have developed. This used activated carbon as the negative electrode and the various EMDs as the positive electrode. Aqueous 2 M NaOH solution was used as the electrolyte. The capacitor achieved 1.6 V corresponding to a capacitance of ~ 50 F g^{-1} of the EMDs from leach liquors. The EMD derived from the synthetic solution showed an inferior capacitance of 25 F g^{-1}. Extended cycling (2000 cycles), showed 100% capacity retention was achieved for one EMD produced from the leach liquor derived from low-grade manganese ore / residue. This outstanding capacitor performance was correlated with the presence of a nanofibrous morphology. These findings open up the possibility of extracting a high performance EMD product from a low cost, low-grade source of manganese.

1. Introduction

The intense interest in manganese dioxide for energy applications is driven by the low cost and non-toxicity of this material when compared with nickel and cobalt oxides [1-2]. The rich chemistry and diverse crystalline structures of manganese dioxides (MnO_2) offer a versatility which allows its use in a range of applications. Manganese dioxides used in batteries and electrochemical capacitors are broadly classified into three groups according to their origin – i.e. natural manganese dioxide (NMD), chemical manganese dioxide (CMD), and electrolytic manganese dioxide (EMD). Despite crystal similarities, NMD, CMD and EMD exhibit different physical and electrochemical properties. The natural ore (NMD) is not a single stoichiometric MnO_2 but, rather, a mixture of up to 10-20 different manganese oxide minerals [3-4] that have widely differing battery activities and inferior battery performance compared to the other two forms (CMD and EMD). The synthesis of CMD involves the chemical oxidation of precipitated Mn(II) from an aqueous solution of $MnSO_4$ [5]. The γ-MnO_2 prepared chemically (CMD) has marginal performance compared to that derived from electrochemical methods (EMD). The latter being widely used in the battery industry. To overcome this, the electrochemically active form of MnO_2 (γ-MnO_2) is prepared by electrodeposition from a very acidic $MnSO_4$ bath at ~ 95° C [5]. This phase is commonly thought of as an intergrowth of pyrolusite in a ramsdellite phase with varying degrees of micro twinning. This EMD phase exhibits the greatest battery and capacitor activity for most applications [6-7]. EMD can be formed from the direct electrolysis of an aqueous bath of manganese sulphate and sulphuric acid.

Numerous reports [8-11] are available regarding the synthesis of EMD from various manganese ores and its use in energy storage applications. The possibility of producing EMD from low-grade and secondary manganese resources has not been fully explored. Production of EMD from a range of sources will be necessary to meet future escalating demand. Owing

to the high demand for EMD used in energy storage applications, there is a need to develop EMD from in-expensive alternate sources of manganese. In our current work, we have identified a different approach to electro-synthesize EMD from different precursors i.e. low-grade manganese residue, manganese cake and a synthetic solution. Manganese cake and leach residue (low-grade) are the side products obtained as waste material from Mn nodule processing [12, 13]. Manganese nodules are metallic clusters which form on the sea floor. These comprise layers of iron and manganese hydroxides. One of the author's home institutions (Institute of Minerals and Materials Technology) has built a hydrometallurgical plant to recover Cu, Ni and Co from manganese nodules [14, 15]. The residue obtained from this process was used as a precursor and more details on the purification of leach liquor can be obtained from Biswal et al. [16]. To the best of our knowledge, use of EMD synthesized from low-grade and secondary manganese sources as a candidate material for use in an asymmetric capacitor (activated carbon *vs*. EMD) has not been reported. If successful, these cost-effective EMD materials might find inexpensive application in large scale energy storage. The work described here investigates the ability of EMD synthesized from different precursors to serve as an electrode material for asymmetric capacitor applications. The characteristics such as improved storage capability, cycling stability, safety and economic life - cycle cost could make the device an attractive alternative to conventional charge storage devices using more expensive high-grade materials. The objective of this work is to study the materials and electrochemistry that influence the electrodeposition of manganese dioxide from the residue Mn(II) liquors or synthetic solution while optimizing the conditions producing high-performance storage ability.

2. Experimental

2.1. Material & methods

Leach liquors were prepared by leaching manganese cake and low-grade manganese residue in a 1 L scale glass reactor at 75 $\pm$ 2 ℃. Initially, 1 L of H_2SO_4 solution at the required concentration (2 M for low grade manganese residue, 1.5 M for manganese cake) was prepared and transferred to the leaching reactor. This was followed by the addition of 100 g of manganese cake and 15 g activated carbon as reductant to produce 10 % (w/v) slurry of manganese cake. Similarly about 200 g of low grade residue and 25 g of activated carbon were taken to prepare a 20% (w/v) slurry of low grade residue. The leaching was continued for 4 h for manganese residue, and 2 h for manganese cake with constant stirring using a Remi stirrer. At the conclusion of leaching, the slurry was cooled, filtered and purified via two stages prior to electrowinning. The purification process for removal of Fe and other trace elements was carried out as detailed in one of our earlier reports [16]. Manganese was estimated volumetrically by EDTA method. The leach liquors were purified and diluted to bring the concentration of manganese to the desired level.

A synthetic (high purity) solution was prepared as an analogue to the leach liquors, by dissolving manganese sulphate in an appropriate concentration of sulphuric acid. All three solutions contained 48 g dm^{-3} manganese as manganese sulfate and 24 g dm^{-3} sulphuric acid.

Electrolytic manganese dioxides (EMDs) was extracted from the three solutions at an anodic current density of 200 A m^{-2} in a glass cell.

Electrodeposition of EMD: Electrodeposition can be defined as the deposition of conductive particles on the substrate from an electrolytic bath by the imposition of current. EMD was deposited at 90 ℃ in an electrolytic cell from the prepared manganese sulfate/sulphuric acid

electrolytes. The anode and the cathode were lead and stainless steel respectively, and current was supplied from a constant current DC source. The deposited EMD was removed mechanically, washed thoroughly and oven dried at 100 ºC. The dried mass was ground and sieved through a 50 µm mesh screen to obtain EMD powder. This powder was washed repeatedly with deionized water until free from sulfate. The washed powder was dried and cooled in a desiccator and then subjected to various physical characterizations.

2.2. Physical Characterization

X-ray diffractograms were obtained from a Phillips Powder Diffractometer (PAN ANALYTICAL PW 1830) using Cu Kα radiation. Scans were recorded in 2θ range $10 - 70$º at 2° per minute. X-ray photoelectron spectra were acquired using a Kratos AXIS Nova spectrometer (Kratos Analytical Ltd, U.K.) equipped with a monochromated Al Kα radiation source (1486.6 eV) operating at 150 W. Survey spectra were recorded at 1 eV/step and a pass energy of 160 eV. Higher-resolution spectra acquired for selected photoemissions were recorded at 0.1 eV/step and a pass energy of 20 eV. The binding energy of the component of the C 1s spectrum attributed to hydrocarbon was measured to be (285.0 ± 0.1) eV for all samples, indicating that there was no accumulation of surface charge during the acquisitions. The morphology and lattice imaging of the EMD materials were characterized by transmission electron microscopy (TEM), high-resolution TEM (HRTEM), electron energy loss spectroscopy (EELS) and high angle angular dark field (HAADF) using a JEOL ARM200F TEM operated at 200 kV. TEM specimens were prepared by grinding a small amount of powder under methanol and dispersing on a holey carbon film. Specimens were examined at liquid nitrogen temperature in a cooling stage, to reduce beam damage and contamination effects.

2.3 Electrochemical characterization

The working electrode consists of active material electrolytic manganese oxide (EMD) or activated carbon (AC) (75 wt %) mixed with carbon black (15 wt %) to improve the conductivity and polyvinylidene fluoride (PVDF) (10 wt %) as a binder. Activated carbon was used as received from Sigma Aldrich with a surface area 1800 m^2 g^{-1}. The composites were suspended in an agate mortar containing 0.3 mL of N-methyl-2-pyrrolidinone (NMP) to form a slurry. A total of 100 µL of slurry was coated on a graphite sheet (geometric surface area of 1 cm^2) and then dried at 60 ℃ for one hour. An aqueous solution of 2 M NaOH was employed as the electrolyte for all electrochemical measurements. For the three-electrode tests, a platinum wire of 10 cm in length and 1 mm in diameter and a mercury-mercuric oxide (Hg/HgO) cell served as the counter and reference electrode, respectively. The asymmetric capacitor was constructed with EMD as the positive electrode and activated carbon as the negative electrode. The electrochemical measurements were carried out using BioLogic VSP-300 instrument. Prior to analysis, initially the electrode was left to equilibrate for 10 min in the electrolyte, and the potential of the working electrode was monitored. This was followed by either cyclic voltammetry or galvanostatic charge-discharge experiments. In the case of potentiostatic electrochemical impedance spectroscopy (EIS) analysis, measurements were made in the frequency range from 1 Hz to 100 kHz with an AC excitation amplitude of 10 mV.

3. Results and Discussion

3.1. Physical characterization of the EMD materials

X-ray diffraction studies

The electrolytic manganese dioxide (EMD) materials obtained from different precursors were characterized by X-ray diffraction (XRD) to reveal the changes in crystal

structure. Figure 1 shows the XRD patterns of the electrodeposited MnO_2 materials. All the peaks of EMD are indexed to γ - MnO_2 on the basis of an orthorhombic unit cell are broad and of low intensity, indicating the formation of poorly crystalline phase and not highly ordered. This is ascribed to non-periodic intergrowth of pyrolusite and ramsdellite structural units [17]. The obtained pattern is in good agreement with the standard values reported in JCPDS card no. 65-1298. The XRD pattern acquired from all the synthesized EMD samples appear to be similar in Fig. 1 and did not reveal any discernible changes between them. This indicates that if the electrolytic deposition parameters are constant then the phases of electrodeposited MnO_2 will be quite similar in crystal structure irrespective of the precursors. To reveal the surface chemical state of manganese and to obtain further information on the composition of the electrodeposited MnO_2, X-ray photoelectron spectroscopy (XPS) was performed.

X-ray Photoelectron Spectroscopy (XPS) studies

A survey spectrum (0–1200 eV) of the surface of EMD obtained from low grade residue is shown in Fig. 2a. Identified in the spectrum are peaks associated with the elements Mn, O, C, and N. The atomic fractions of these elements for each EMD material obtained are listed in Table 1.

Spectra recorded at higher energy resolution for the Mn 2p and 3s regions for the low-grade residue are show in Figs 2b and d, respectively. The Mn $2p_{3/2}$ fitting curves are shown in Fig. 2c. Those acquired from the other samples are similar, and so not presented here. On initial inspection, these spectra are characteristic of MnO_2. The apex of the Mn $2p_{3/2}$ peak has the distinctive shape observed for MnO_2, but not for the oxides of Mn in other oxidation states [18-22], and is centred at 642.3 eV, which is within the range reported for MnO_2. The energy separation between the two components of the Mn 3s peak, arising from coupling in

the photo-excited ion between the unpaired 3s and 3d electrons, is 4.5 eV, which is also characteristic of Mn(IV) [23].

The Mn 2p spectra of Mn(II), Mn(III), and Mn(IV) compounds are generally broad and asymmetric, as each is a composite of several peaks (multiplets) arising from coupling, in the excited state, between the unpaired 2p and 3d electrons. The theoretical splitting for each state has been calculated by Gupta and Sen [24, 25], and their results applied to the spectra of Mn oxides by Nesbitt and Banerjee [23] and Biesinger et al. [22]. Both observed, in the Mn 2p spectra acquired from MnO_2, a low binding energy component to the Mn $2p_{3/2}$ peak that they could not assign to a multiplet peak of Mn(IV). Instead, this component was attributed to contributions from Mn(III) [22, 23] and, by Nesbitt and Banerjee only, Mn(II) [21]. A similar shoulder is present in the Mn 2p spectra acquired from the EMD samples. The relative contribution of the shoulder to the overall peak area was around 15% for all samples. The general trend is the same for all fitting methods. The ratio of Mn(III) to Mn(IV) is approximately the same for all the samples regardless of the precursors. Furthermore, from the fits obtained for the Mn 2p spectra, it seems likely that the O 1s spectra would be matched by contributions from O atoms in Mn(III), as well as Mn(IV), coordination. Each C 1s spectrum (in Fig. 2e) was fitted to three components. The most intense of these is the component at the lowest binding energy, which is attributed to carbon atoms in hydrocarbon groups. The binding energies of all spectra were shifted so that this component was centred at 285.0 eV, to correct for energy shifts resulting from sample charging during irradiation. The binding energy of the second component in each C 1s spectrum is 1.6 - 1.7 eV higher than that of the hydrocarbon peak, and so is attributed to carbon atoms singly bonded to oxygen, in either alcohol or ether functional groups. The binding energy of the third component is between those generally observed for C=O and O-C=O functional groups, and is possibly a composite of contributions from both. The binding energies and relative contributions of each

component are listed in Table 1. The XPS spectra acquired from all the electrodeposited EMD samples were similar and did not appear to have any distinct differences between them, the confirmation of Mn(IV) oxidation state. Nevertheless, the proportion of Mn(IV) could be slightly higher relative to that of Mn(III) or Mn(II) for low-grade residue as compared to that of derived from the cake and synthetic solutions. This can be inferred from the lengthening of the average Mn – O bonds (see Table 1) with an increased surface area. A possible correlation is suggested between the electrochemical reactivity and the surface area of the active "OH" groups. The BET surface areas of the EMD samples were calculated to be 104, 100 and 55 m^2 g^{-1} for low-grade, cake and synthetic solution-derived materials, respectively.

Transmission electron microscopy (TEM) studies

The particle size of the electrodeposited MnO_2 derived from low-grade residue was quite fine (Fig. 3a). It was composed of aggregates of small crystallites with a relatively uniform grain size of about 7 nm. Examination of a number of other regions of the powder sample containing particulates suggested that they were all quite similar (not shown). Energy dispersive x-ray spectroscopy (EDS) of these particles (not shown) confirmed that they contained just Mn and O. The high resolution TEM imaging showed lattice fringes with an interplanar spacing of ~ 0.8 nm (Fig. 3b) corresponding to the typical interplanar spacing of (101) plane of EMD type $\gamma – MnO_2$. Fig. 3c shows a high angle annular dark field (HAADF) scanning TEM image, which is highly sensitive to atomic number contrast. This region shows a fine scale and fibrous particle and in this region electron energy loss spectroscopy (EELS) had been performed (Fig. 3d). The incident electron loses energy as it traverse the specimen, due to various electronic transitions. This results in fine structure within the spectrum, from which the determination of valence state is possible. In the case of Mn, the Mn $L_{2,3}$ peaks appear as a doublet. The relative intensities of these peaks, and especially the fine structure in the O K edge at 532eV, vary as a function of valence state. Comparison with library and

published spectra for this phase strongly suggests that it is MnO_2 and that the Mn is in the 4+ state Riedl et al [26]. The high resolution of fibrous particle (not shown) suggested that the particle is crystalline with a granular region. The fibrous structure could provide effective active sites while facilitating the mobility of ionic diffusion [27]. The TEM imaging observed for the Mn cake as precursor (Fig. 4) is quite similar in morphology with homogeneity and densely packed, as compared to that of low grade residue (Fig. 3a). Figs. 4a,b show rice grain-shaped coarse particles with a grain size of about 10-20 nm and a very fine grained phase. The high resolution TEM imaging (Fig. 4c) shows a nanocrystalline region leading to a large surface area and rich porous structure for energy storage. In the case of the EMD derived from the synthetic solution (Fig. 5), although the morphology looks similar to that of low grade and cake (Figs. 3 and 4), closer examination reveals spindle-shaped particles of over 1 μm in length (Fig. 5b). The HAADF imaging (Fig. 5d) shows a similar pattern of large particles. High resolution TEM imaging (Fig. 5c) lattice fringes show crystallinity with a long rod-shaped particles evident. This implies that the morphology of EMD derived from the synthetic solution is quite different to that of EMD derived from the two leach liquors (low-grade and cake). This spindle-shaped agglomerated particles result in a lower surface area (55 $m^2 g^{-1}$) as detailed in the previous section [28].

3.2   Electrochemical characterization of the EMD materials

Single cell characteristics

To evaluate the electrochemical properties and quantify the energy storage (specific capacitance) of the electrodeposited EMD materials and activated carbon (as - received), we have performed cyclic voltammogram and charge-discharge measurements on these two-electrodes individually in a 2 M NaOH electrolyte using a three-electrode system. Figure 6a shows the first cyclic voltammogram (CV) of EMD obtained from different precursors under

the conditions noted in the figure. The potentials have been kept within a safe window of operation, to avoid any manganese dissolution or oxygen evolution at the respective low and high potentials. As can be seen in Fig. 6a, the CV profiles for the low-grade and cake exhibits a quasi-rectangular curve without any indication of redox peaks [29]. This illustrates a capacitive - like (non-Faradaic) behaviour with the reversible adsorption and desorption of OH^- ions from/to the electrolyte during the anodic and cathodic processes respectively. However, a smaller contribution from the extraction and insertion of Na^+ cation from/to the EMD bulk corresponding to a faradaic reaction, pseudo capacitance (Cp) associated with charge-transfer resistance (Rct) have not been ruled out. For the synthetic sample the area bounded by the curve is very small compared with the other materials, showing it is not electrochemically active. Moreover, the CV curve of both the low - grade residue and cake - derived EMDs exhibit a nearly symmetric current response. On reversing the scan cathodically, a good reversible behavior indicates that the material is electrochemically viable for charge storage applications. Figs. 6b-c show the changes in the CV profile as a function of different scan rates for low-grade residue and cake-derived EMD respectively. It is worth mentioning here that, a similar current response and shape have been observed for the MnO_2 reported in the literature for aqueous capacitors [29 – 30]. The integrated areas of the CV profile (in Fig. 6b) are proportional to the sweep rates (1, 2, 5 and 10 mV/s) illustrate the electrochemical utilization of MnO_2 is enhanced through the fast redox reactions. This exhibit the low-grade residue material is suitable for high power applications. The almost symmetric quasi-rectangular shape of the CV curves (in Fig. 6b) and the large current response showed reversible and strong capacitive behavior for low-grade residue derived EMD. The EMD derived from cake (in Fig. 6c) shows sustainable behaviour only at lower scan rates (<10 mV/s). At higher scan rates (10 mV/s) the shape of the curve changes from quasi-rectangular to elliptical. A very similar response is observed for TiO_2 nanotube films when used as

electrodes for capacitors [31]. It appears that the cake-derived EMD deviates from the ideal

capacitive behavior at high scan rates. The lack of symmetry of the CV curves (in Fig. 6c)

could be due to the lower electrical conductivity of cake-derived EMD and the slower

diffusion rate inside the available pores that resulting in a decreased current response [31-32].

The decay of performance with increasing scan rate reflects the mass transfer kinetic

limitations on the electrode surface. The CV testing at higher scan rates was not performed

for EMD derived from synthetic solution, as the performance at low scan rate was not

comparable to that of the other materials. From these preliminary electrochemical studies, it

is concluded that the useful and safe voltage window for EMD operation is 0 - 0.6 V.

The CV profile of the activated carbon (AC) negative electrode is shown in Fig. 7.

The CV exhibits a nearly ideal rectangular shape, and no redox peaks are observed. The inset

in Fig. 7 at a lower scan rate (1 mV/s) indicates a typical characteristic of electrochemical

double layer capacitor (EDLC) behavior [33-34]. The cations and anions from the NaOH

electrolyte are adsorbed on the activated carbon layer during the anodic process while they

are desorbed during the reverse scan [33, 30]. With increasing scan rate, the shape of CV is

gradually distorted from rectangular to elliptical. At higher scan rates, the material is still

reversible with an excellent current response but the distorted shape of CV curve implies

sluggish OH$^-$ ion transport from the electrolyte to the carbon electrode is being limited on the

surface rather in the bulk. This sort of EDLC behaviour at a lower scan rate for activated

carbon is quite typical and is therefore suitable to act as a negative electrode with a useful

operating voltage of 1 V. On the basis of these results, we can see in Fig. 8a that the stable

voltage for activated carbon is 1 V (-1.0 V to 0 V) and for EMD (low grade residue) is 0.6 V

(0 V to 0.6 V) with a scan rates between 2 and 5 mV/s. Therefore, for a cell containing

activated carbon *vs.* EMD, the safe operating cell voltage could be 1.6 V in 2 M NaOH

electrolyte. The specific capacitances of each electrode were calculated by galvanostatic

discharge-charge measurements as shown in Fig. 8b. The EMD electrode potential increases

from 0 to 0.6 V upon charging while that of the activated carbon electrode varied from 0 to -

1.0 V. The specific capacitance of the active material EMD and AC after subtracting from

contributions of carbon black (acetylene black) and binder were calculated to be 75 F g^{-1} and

110 F g^{-1} respectively. It is quite common to use carbon black as an additive [35-36] in the

EMD cathode, to reduce interparticle contact resistance and enhance the electrical percolation

network with improved electronic conductivity. To avoid any discrepancy (like irreversible

cell capacitance) arises from the carbon black, only the active material has been taken into an

account for calculating specific capacitance. Based on the single cell characteristics, to

maintain the charge balance of the hybrid cell, the weight ratio between the negative and

positive electrodes ($k = m_+/m_-$) was estimated to be 2.44.

Asymmetric device (activated carbon vs. EMD)

Galvanostatic charge/discharge experiments were carried out for the asymmetric capacitor

(Figs. 9 - 10). Figs. 9 a-c show typical charge – discharge curves of the asymmetric device

with a voltage window of 1.6 V tested at a current of 2 mA for the EMD samples obtained

from low grade residue, cake and synthetic solution respectively. A typical near-symmetrical

shaped charge-discharge curve indicates pure capacitive behaviour, however, resistances in

the electrode-electrolyte system lead to a slight deviation from the ideal system, causing an

inflection at higher (1.6 V) and lower voltage (0.0 V). Among the three precursors (Fig. 9a-c)

the EMD derived from low-grade residue (Fig. 9a) and manganese cake (Fig. 9b) displayed

the highest capacitance of 50 F g^{-1} while that derived from the synthetic solution delivered

just half of that value, 25 F g^{-1} during the initial cycle. This can be ascribed to the low grade

and cake having relatively higher surface area, similar particle size and fibrous phase

morphology. The enlarged specific surface area and the presence of fibrous phase ensure

sufficient exposure of the EMD to the aqueous NaOH electrolyte. The presence of spindle-

shaped particles in the EMD derived from the synthetic solution and the differences observed in the chemical state of Mn through XPS could be attributed to the lower specific capacitance. The asymmetric device has shown excellent cycling stability performed in the voltage window of 1.6 V at a current density of 2 mA and the capacity retention plots are shown in Fig.10. It is quite interesting to note that, excellent capacity retention of almost 100% was maintained for EMD derived from low grade residue after 2000 cycles while that derived from cake lost 11 F g^{-1} from the initial value with retention of only 80% after 2000 cycles. In the case of EMD derived from the synthetic solution, the initial capacitance was fairly low of 25 F/g and a capacity of 80% was retained after 2000 cycles. An asymmetric capacitor using EMD from low-grade residue is capable of delivering energy density of 17 Wh kg^{-1} at a power density of 400 W kg^{-1}. The values observed in the present study are comparatively higher than the reported values for MnO_2 *vs.* activated carbon and graphene based systems [29-30, 37-40] but lower to the graphene oxide (GO) − based MnO_2 composite systems [39, 41-42], as shown in Table 2. The reported larger capacitance values in the previous reports [39, 41-42], tabulated in Table 2, are mainly originated from typical synthetic route such as reduced graphene oxide (rGO) as a composite in MnO_2 material. Although rGO-MnO_2 composites and adding surfactant in MnO_2 possess a porous structure for electrolyte access and effective larger surface area but it is obtained at the expense of stringent synthetic conditions. In our case, a cost-effective, low grade residue and activated carbon have been used as electrodes which can offer an inexpensive energy storage device.

The Nyquist plot of EMD derived from low-grade residue before and after cycling experiments is shown in Fig. 11A. The electrochemical impedance spectroscopy (EIS) spectra for the samples before and after electrochemical cycling shown in Fig. 11A are quite similar in terms of the shape of the curve obtained but a change in equivalent series resistance is observed, shown in Table 3. The Nyquist plot based on the equivalent circuit is displayed

in Fig. 11B. The absence of semicircular plot in the high frequency range implies low interfacial resistance of the material which is a typical capacitor behavior [43]. However, a depressed semicircle is seen for the fresh sample followed by a linear part in the low frequency region which is a nature of pure capacitive behavior. The sloping linear part for the fresh sample indicates diffusion in active electrode material and electrolyte interface. The semicircle in Nyquist plot is described by a parallel circuit of R_{ct} (charge-transfer resistance) and C_{dl} (double layer capacitance) while C_p (pseudo capacitance) is for the steep inclined line. For fitting purposes, we replaced C_{dl} with a constant phase element (CPE) by including the physicochemical properties of the EMD electrode. The intersection of the semicircle on the real axis represents the equivalent series solution resistance (R_s) of the EMD electrode, and the diameter of the semicircle corresponds to the R_{ct} of the EMD electrode and aqueous NaOH electrolyte interface [44]. The R_{ct} is controlled by the kinetics of the electrochemical reactions and the diffusion of ions near the EMD surface. After 2000 cycles, two characteristics of the Nyquist plot can be observed, one is the electrochemical resistance increases from an initial value of 22.6 to 40.1 Ω cm^2 (see Table 3) indicating a good conductivity of the aqueous electrolyte is maintained after multiple cycles. The other factor is only a marginal increase (from 17.3 to 20.6 Ω cm^2) in charge-transfer resistance reflecting good electronic conductivity of the material is maintained after the cyclability and therefore the capacity retention is quite high. Another element from the equivalent circuit is Warburg impedance (W), appeared at a low frequency on the Nyquist plot in Fig. 11A. An inclined line, Warburg portion, for the cycled sample has lower Warburg impedance (1.3 Ω s$^{-1/2}$) that is attributed to the dynamics of particle diffusion in a concentration gradient resulting in build-up of diffusion layer. The slope of the inclined line confirms the faradaic (C_p and R_{ct}) and non-faradaic behaviour (C_{dl}) of the EMD material. The pseudocapacitance (C_p) of the

electrodes before and after cycling is similar to those values obtained from the experimental value (in Fig. 10) confirms the reliability of the fitting parameters.

Conclusions

Electrodeposited MnO_2 (EMD) produced from different precursors has been investigated for use in an aqueous electrolyte-based assymetric capacitor. XPS and electron energy loss spectroscopy showed the manganese to be predominantly in +4 oxidation state regardless of the precursors used. However, different morphologies were observed for the three different types of EMD tested and changes in Mn-O bonding have been identified for EMD derived from the synthetic solution, when compared with the other materials. The capacitor using EMD as a positive and activated carbon negative electrode has been fabricated using aqueous NaOH solution as an electrolyte. EMD derived from low-grade and cake precursors exhibited the highest capacitance 50 F g^{-1} and an energy density of 17 Wh kg^{-1}. In contrast, the EMD derived from the synthetic solution produced a capacitance of 25 F g^{-1} and an energy density of 9 Wh kg^{-1}. The device constructed with EMD derived from low-grade residue showed excellent capacity retention while the cake and synthetic samples lost 20% of the initial capacitance after 2000 cycles. The enhanced performance is attributed to a larger surface area, unique morphology and strong Mn – O bonds.

Acknowledgements

References

1. W. M. Dose, J. Lehr and S. W. Donne, Mater. Res. Bull., 2012, **47**, 1827-1834.

2. R.M. Dell, Solid State Ionics, 2000, **134**, 139-158.

3. H. Adelkhani, M. Ghaemi, Solid State Ionics, 2008, **179,** 2278-2283.

4. R. Huber, in Batteries, Vol. 1, Manganese Dioxide, K.V. Kordesch, Marcel Dekker (Eds.), New York, 1974, Chapter 1.

5. J. Prabhaker and S. Viswanathan, J. Power Sources, 1993, **42**, 335-343.

6. A. Kozawa, in Batteries, Vol. 1, Manganese Dioxide, K.V. Kordesch, Marcel Dekker (Eds.), Springer, New York, 1974, 385 – 519.

7. M. Minakshi, P. Singh, T. B. Issa, S. Thurgate and R. DeMarco, J. Power Sources, 2004, **130,** 254-259.

8. O. Schilling and J. R. Dahn, *J. Appl. Crystallogr.*, 1998, **31**, 396-406.

9. A. G. Kholmogorov, A. M. Zhyzhaev, U. S. Kononov, G. A. Moiseeva and G. L. Pashkov, Hydrometallurgy, 2000, **56,** 1-11.

10. H. Malankar, S. S. Sharma, K. Singh and M. Sharma, J. Solid State Electrochem., 2010, **14**, 71-82.

11. R. N. Sahoo, P. K. Naik, and S. C. Das, Hydrometallurgy, 2001, **62**, 157-163.

12. A. Biswal, K. Sanjay, M. K. Ghosh, T. Subbaiah, and B. K. Mishra, Hydrometallurgy, 2011, **110,** 44-49.

13. A. Biswal, B. C. Tripathy, K. Sanjay, T. Subbaiah, and M. Minakshi, RSC Adv., 2015, **5,** 58255-58283.

14. R.P. Das, S. Anand, *Proc. ISOPE Ocean Mining Symp.*, Seoul, **1997,** 165–171.

15. N.K. Mittal, P.K. Sen, *Minerals Engin.* 2003, **16**, 865-868.

16. A. Biswal, B. C. Tripathy, K. Sanjay, D. Meyrick, T. Subbaiah and M. Minakshi, J. Solid State Electrochem., 2013, **17,** 3191-3198.

17. J. E. Post, Proc. Natl. Acad, Sci USA, 1999, **96** (30) 3447-3454.

18. M.A. Stranick, Surf. Sci. Spectra, 1999, **6**, 31-38.

19. M.A. Stranick, Surf. Sci. Spectra, 1999, **6**, 39-46.

20. M.C. Militello and S.W. Gaarenstroom, Surf. Sci. Spectra, 2001, **8,** 200-206.

21. H.W. Nesbitt and D. Banerjee, Am. Mineral., 1998, **83,** 305-315.

22. M.C. Biesinger, B. D. Payne, A. P. Grosvenor, L. W. M. Lau, A. R. Gerson and R. C. Smart, Appl. Surf. Sci., 2011, **257,** 2717-2730.

23. Thermo Scientific XPS Knowledge Base, Manganese.

http://xpssimplified.com/elements/manganese.php

24. R.P. Gupta and S.K. Sen, Phys. Rev. B, 1974, **10**, 71-77.

25. R.P. Gupta and S.K. Sen, Phys. Rev. B, 1975, **12**, 15-19.

26. T. Riedl, T. Gemming and K. Wetzig, Ultramicroscopy, 2006, **106**, 284-291.

27. E. S. Pampal, E. Stojanovska, B. Simon and A. Kilic, J. Power Sources, 2015, **300**, 199-215.

28. S.-L. Yang, R.-G. Ma, M.-J. Hu, L.-J. Xi, Z.-G. Lu and C. Y. Chung, J. Mater. Chem., 2012, **22**, 25402-25408.

29. M. Vedi Kuyil Azhagan, M. V. Vaishampayan and M. V. Shelke, J. Mater. Chem., 2014, **2**, 2152-2159

30. M. Huang, Y. Zhang, F. Li, L. Zhang, R. S. Ruoff, Z. Wen and Q. Liu, Sci. Rep., 2014, **4**, 3878-3884

31. M. Zhou, A. M. Glushenkov, O. Kartachova, Y. Li and Y. Chen, J. Electrochem. Soc., 2015,**162**, A5065-A5069.

32. K. Zaghib, J.B. Goodenough, A. Mauger and C. Julien, J. Power Sources, 2009, **194**, 1021-1023.

33. J. Xu, Q. Gao, Y. Zhang, Y. Tan, W. Tian, L. Zhu and L. Jiang, Sci. Rep., 2014, **4**, 5545-5550.

34. S. Majumder, S. Dey, K. Bagani, S. K. Dey, S. Banerjee and S. Kumar, Dalton Trans., 2015, **44**, 7190 – 7202.

35. X. Qi, B. Blizanac, A. DuPasquier, P. Meister, T. Placke, M. Oljaca, J. Li and M. Winter, Phys. Chem. Chem. Phys. 2014, **16**, 25306 – 25313.

36. M. Manickam and M. Takata, J. Power Sources, 2002, **112**, 116 – 120.

37. T. Brousse, P.-L. Taberna, O. Crosnier, R. Dugas, P. Guillemet, Y. Scudeller, Y. Zhou, F. Favier, D. Belanger and P. Simon, J. Power Sources, 2007, **173**, 633-641.

38. I.-T. Kim, N. Kouda, N. Yoshimoto and M. Morita, J. Power Sources, 2015, **298**, 123-129.

39. C. J. Jafta, F. Nkosi, L. le Roux, M. K. Mathe, M. Kebede, K. Makgopa, Y. Song, D. Tong, M. Oyama, N. Manyala, S. Chen, and K.I. Ozoemena, Electrochim. Acta, 2013, **110**, 228-233.

40. P. Staiti and F. Lufrano, Electrochim. Acta, 2010, **55**, 7436 - 7442.

41. H. Chen, S. Zhou, M. Chen and L. Wu, J. Mater. Chem., 2012, **22**, 25207-25216.

42. P.Y. Chan and S. R. Majid, Solid State Ionics, 2014, **262**, 226-229.

43. H. Pang, Y. Ma, G. Li, J. Chen. J. Zhang, H. Zheng and W. Du, Dalton Trans. 2012, **41**, 13284 – 13291.

44. Q. Cheng, J. Tang, J. Ma, H. Zhang, N. Shinya and L. C. Qin, Carbon, 2011, **49**, 2917 – 2925.
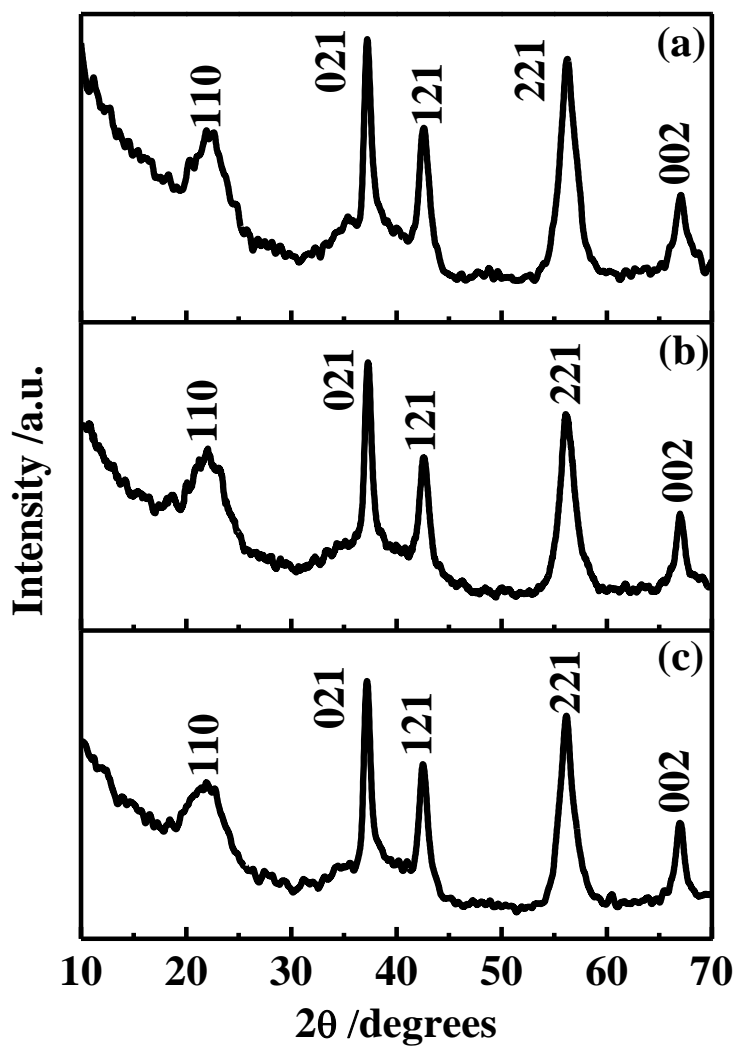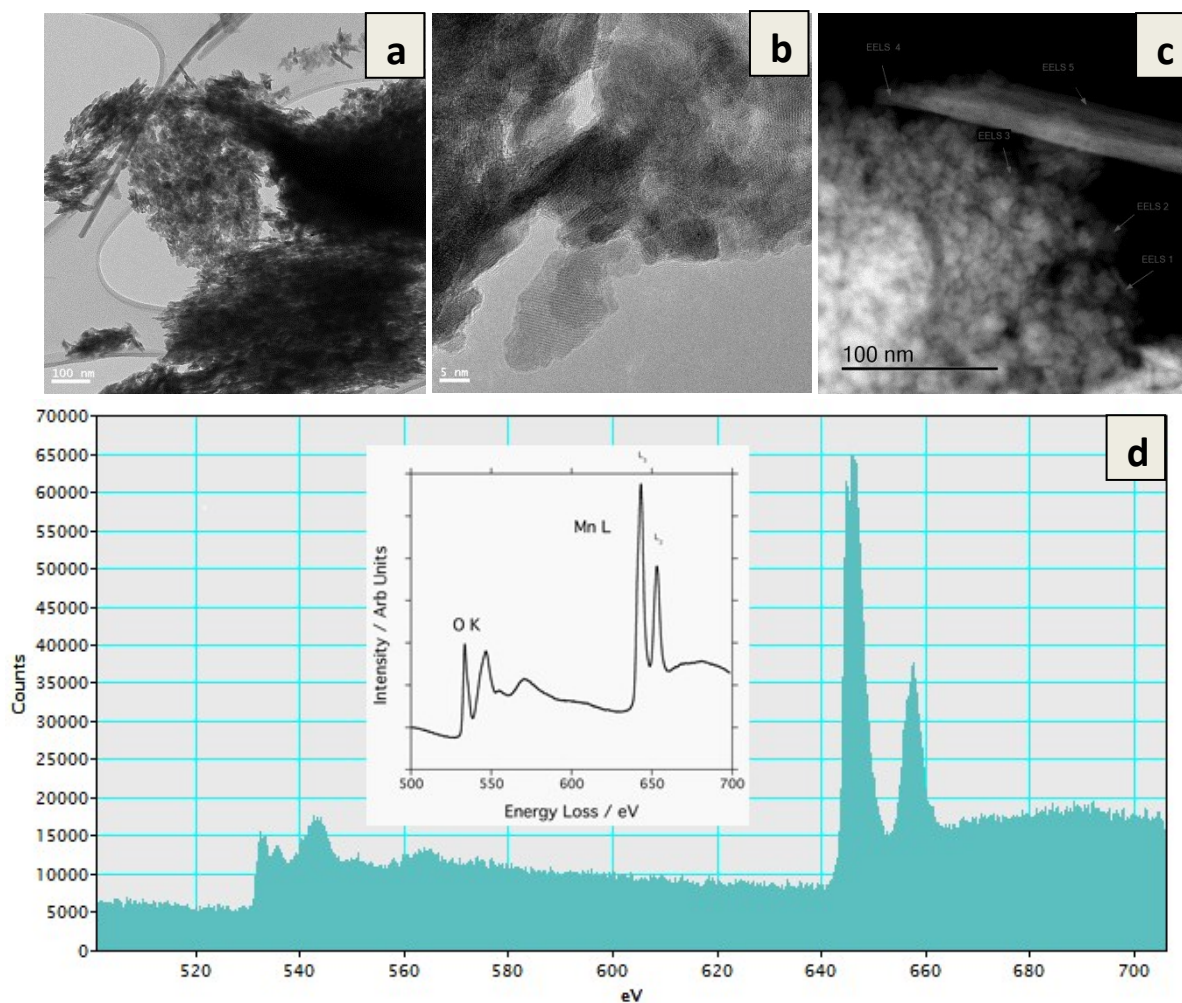

Figure 1 X-ray diffraction (XRD) patterns of the EMD materials derived from precursors (a) low-grade residue, (b) manganese cake and (c) synthetic solution.
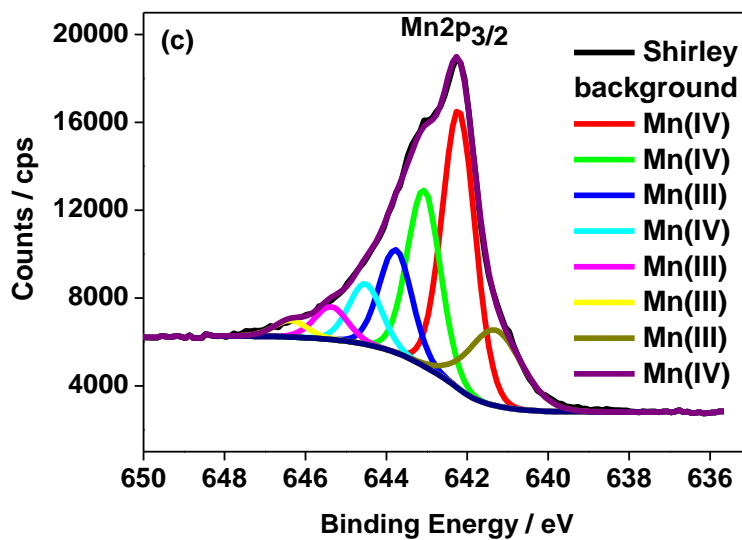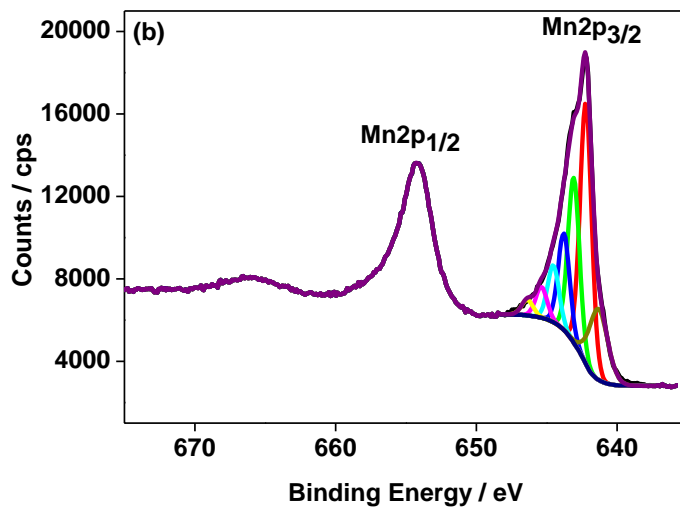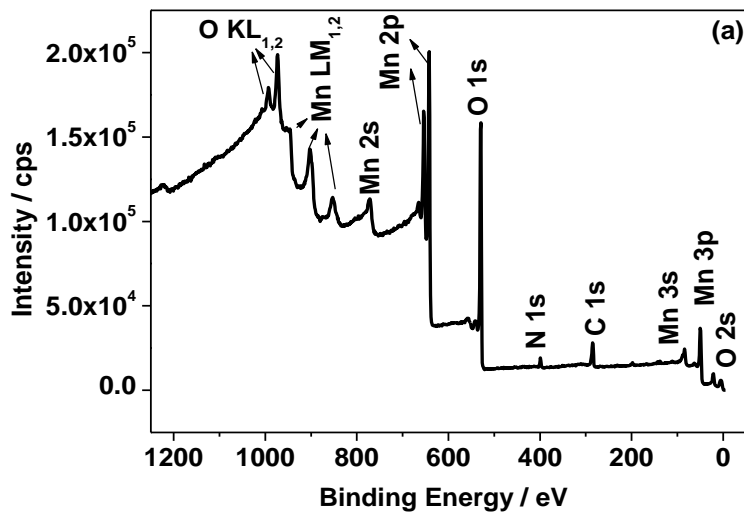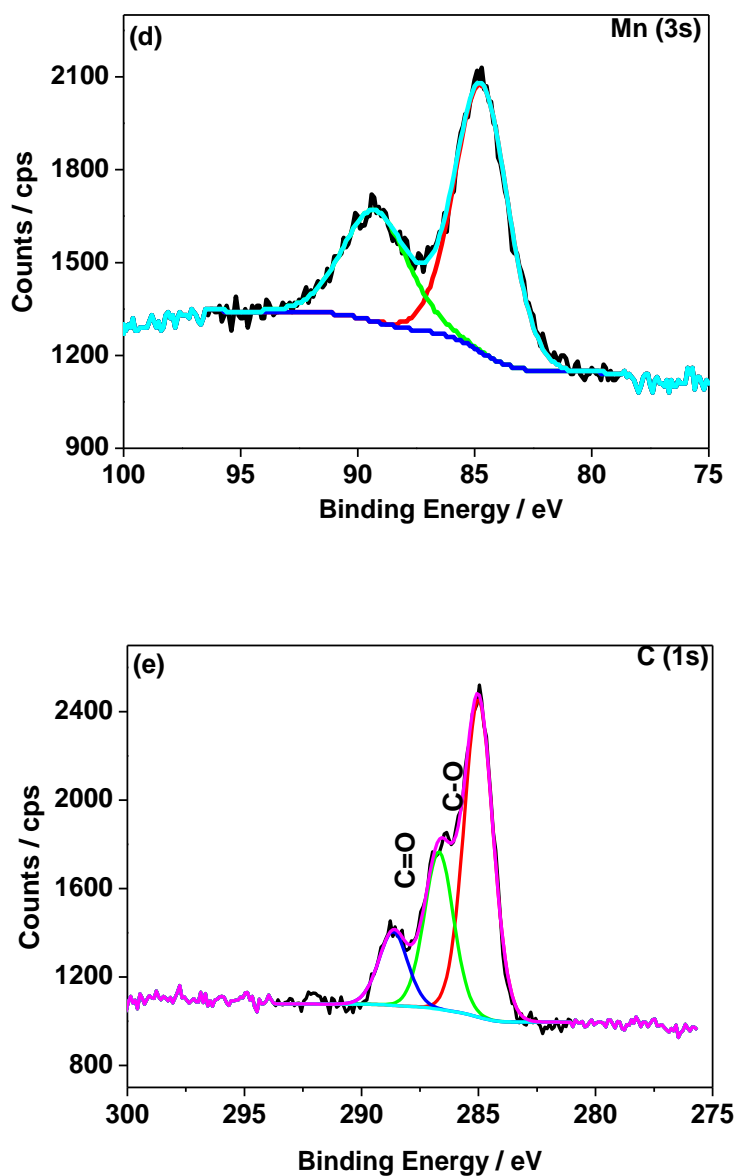
Figure 2 X-ray photoelectron spectroscopy (XPS) spectra (a) wide scan region, (b) Mn *2p*, (c) Mn *2p*$_{3/2}$ fitting, (d) Mn *3s*, and (e) C *1s* deconvolution peaks for EMD (γ-MnO$_2$) samples derived from low-grade residue.

Figure 3 (a) Low magnification bright-field TEM image, (b) high resolution TEM (HRTEM), (c) high angle-annular dark field (HAADF) TEM image of fibrous structure and (d) corresponding electron energy loss spectroscopy (EELS) for EMD (γ-MnO₂) samples derived from low-grade residue. Inset is the typical EELS spectrum for EMD.
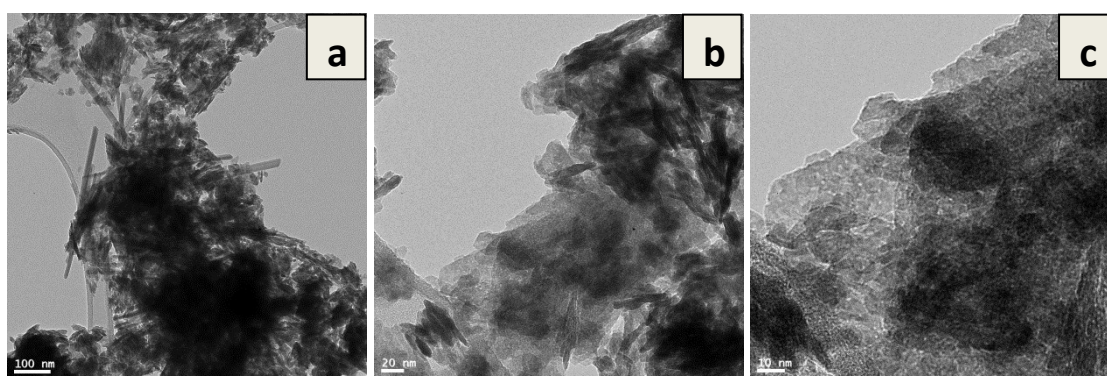

Figure 4 (a-b) Low magnification bright-field TEM, (b) detailed image of the individual particle showing rice grain shape, and (c) high resolution TEM (HRTEM) for EMD (γ-MnO₂) samples derived from manganese cake.

22
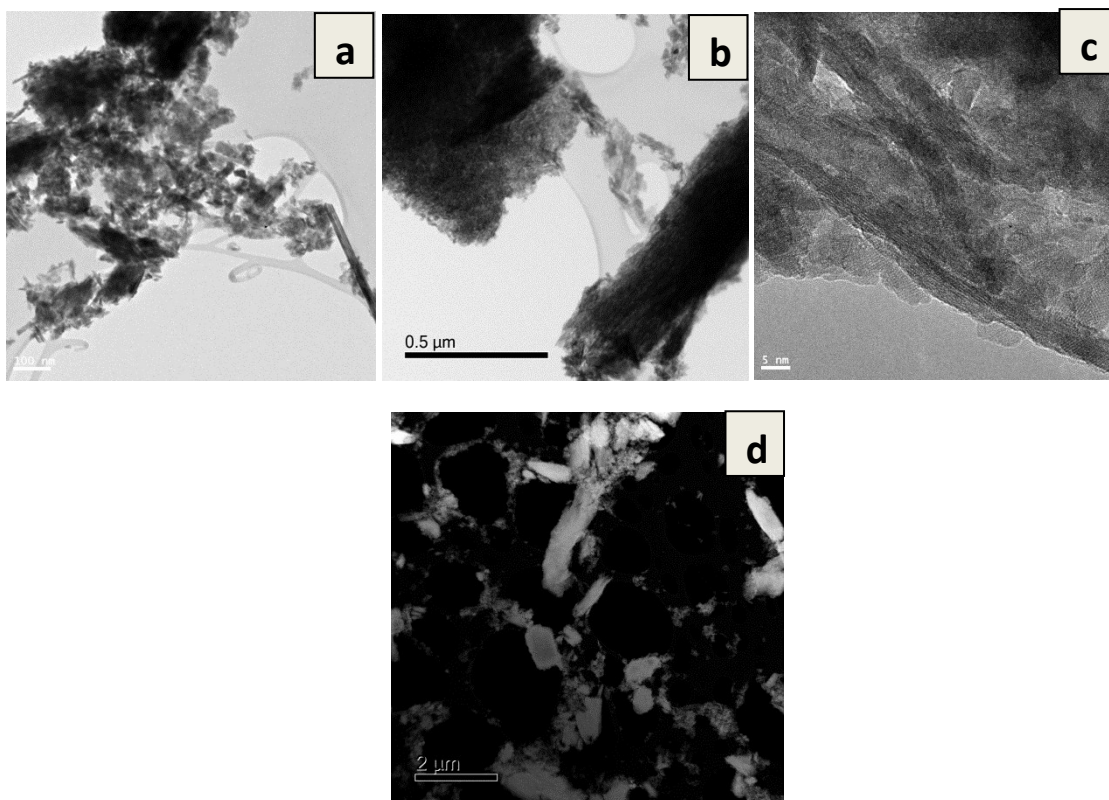
Figure 5 (a) Low magnification bright-field TEM, (b) detailed image of the individual particle showing spindle shape, (c) high resolution TEM (HRTEM) of the spindle shaped particulate and (d) high angle-annular dark field (HAADF) TEM image for EMD (γ-MnO_2) derived from synthetic solution.
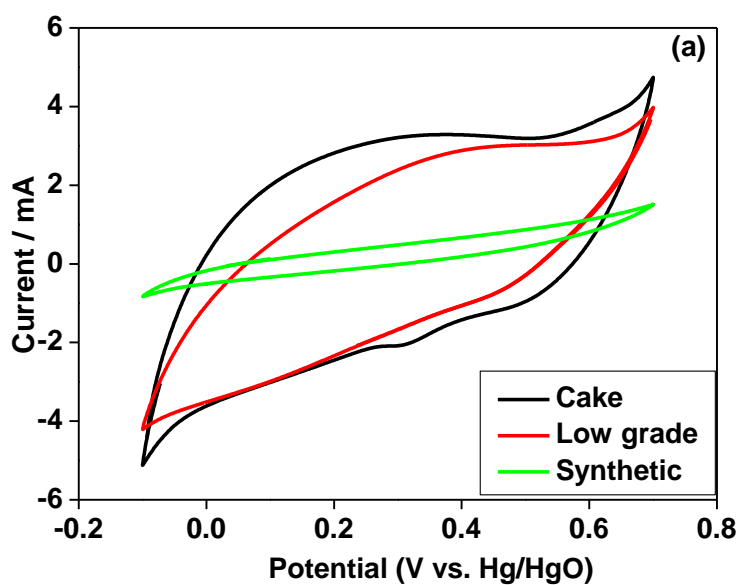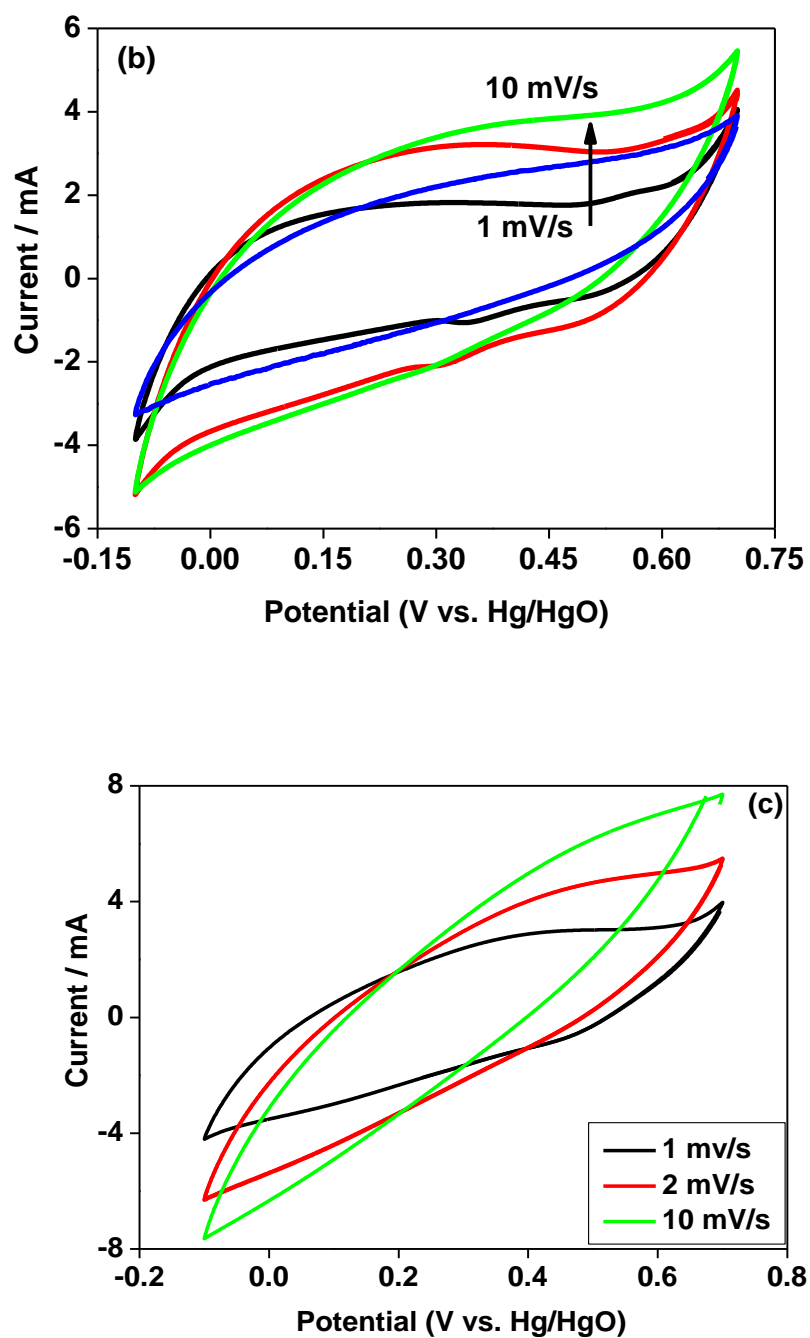
Figure 6 Cyclic voltammogram (CV) measurements of (a) EMD derived from different precursors at 2 mV/s; The effect of scan rate on: b) EMD derived from low-grade residue, and (c) EMD derived from cake. Experiments were performed in a three-electrode system in 2M NaOH electrolyte.
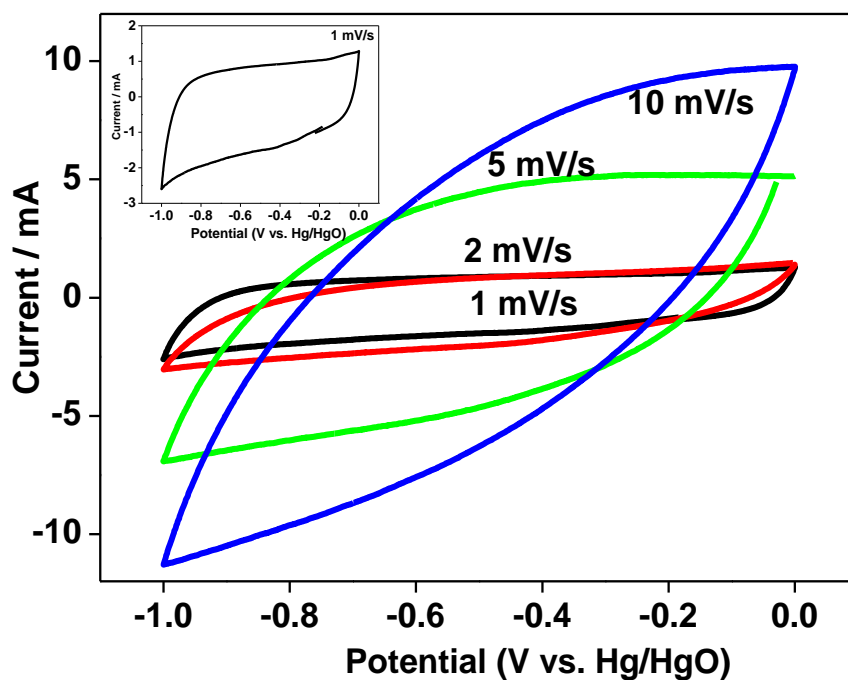
Figure 7 Cyclic voltammogram (CV) measurements of activated carbon at different scan rates. Inset is the typical electrochemical double layer capacitor (EDLC) behaviour at a low scan rate of 1 mV/s. Experiments were performed in a three-electrode system in 2M NaOH electrolyte.
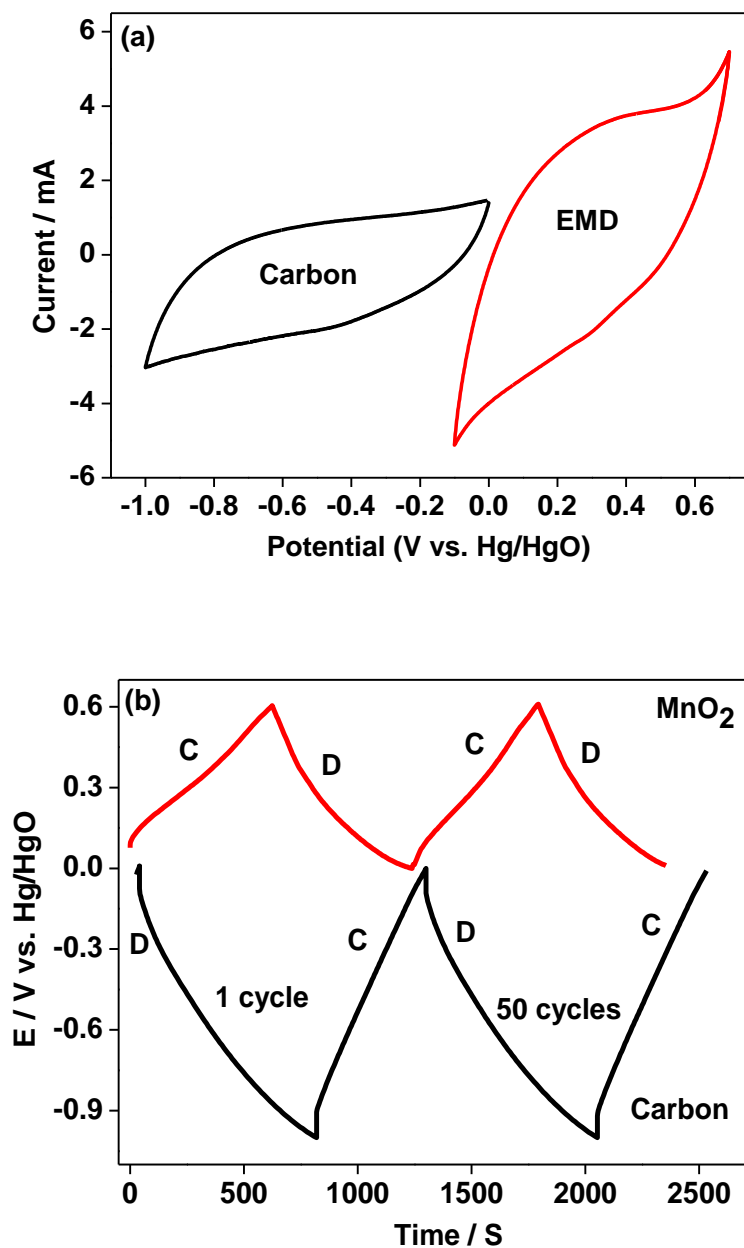
**Figure 8** (a) Cyclic voltammogram (CV) curves for activated carbon (AC) negative electrode and EMD positive electrode at 2 mV/s and (b) corresponding galvanostatic (charge-discharge) curves for each electrode at 2 mA. The plots are shown for the 1st and 50th cycles. Experiments are performed in a three-electrode system in 2M NaOH electrolyte. (Terms C and D referes to charge and discharge, respectively).
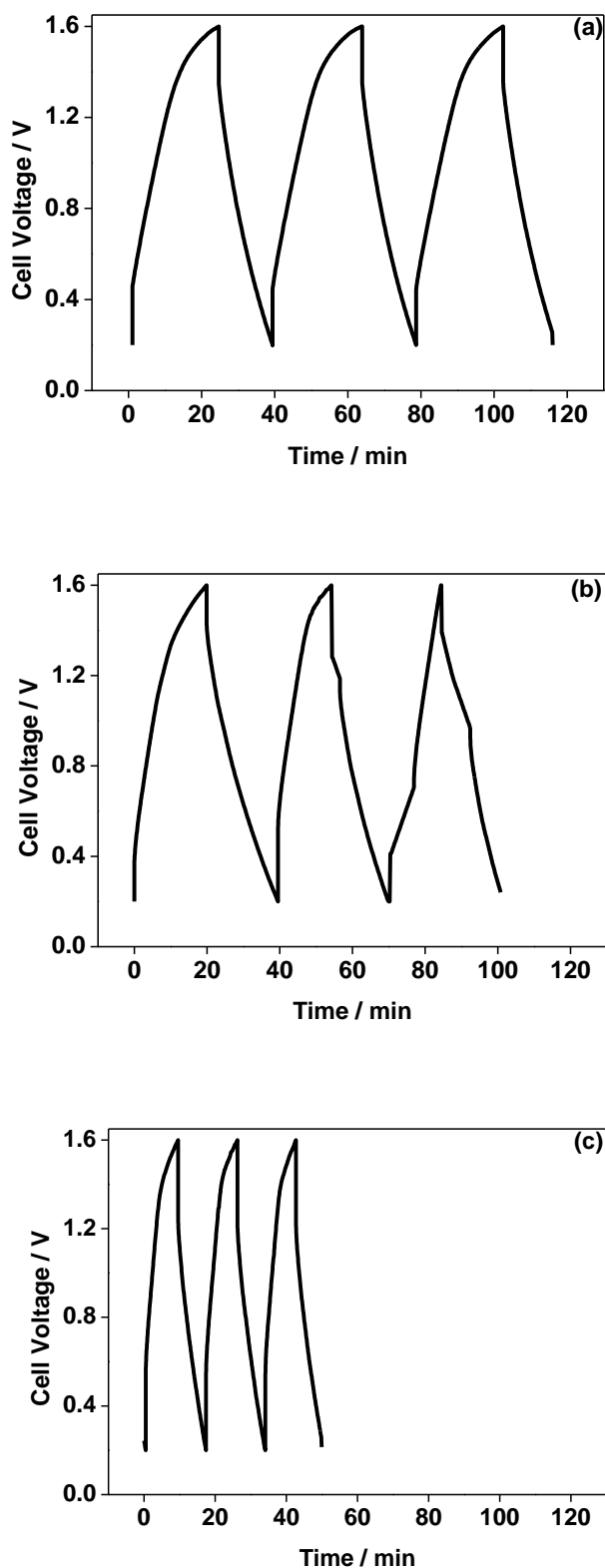
Figure 9 Charge-discharge voltage profile of the activated carbon vs. EMD asymmetric capacitor. EMD derived from (a) low-grade residue, (b) manganese cake, and (c) synthetic solution measured at a constant current of 2 mA in 2M NaOH electrolyte. Plots are shown for the 1, 300 and 500 cycles. The EMD derived from the low grade residue (a) shows the best performance.
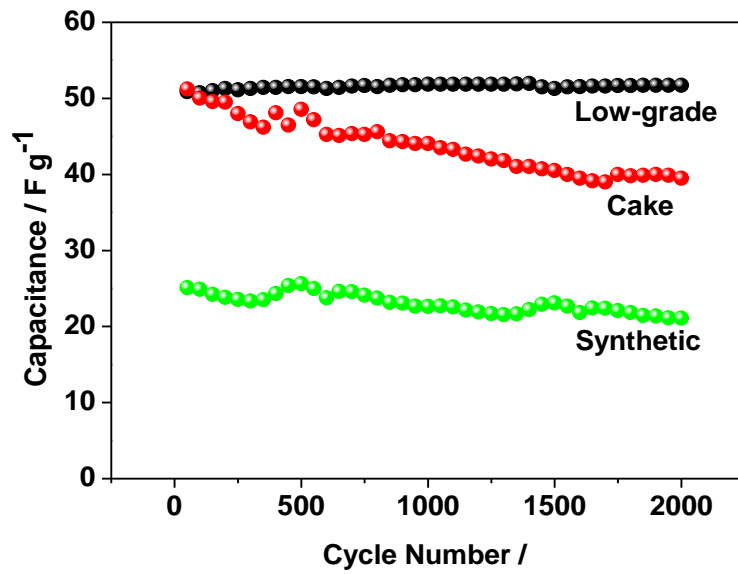
Figure 10 Cycling performance of the activated carbon vs. EMD asymmetric capacitor. EMD derived from different precursors are shown, after 2000 cycles the capacity retention is superior for low grade residue.

(A)

28
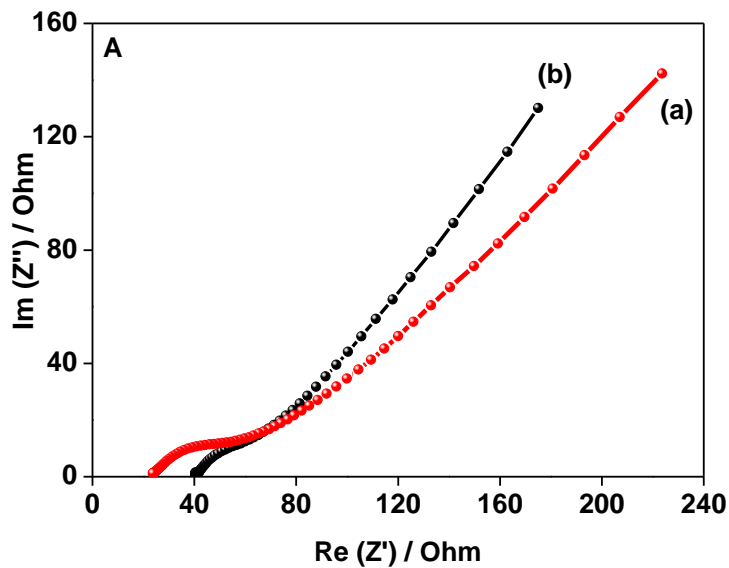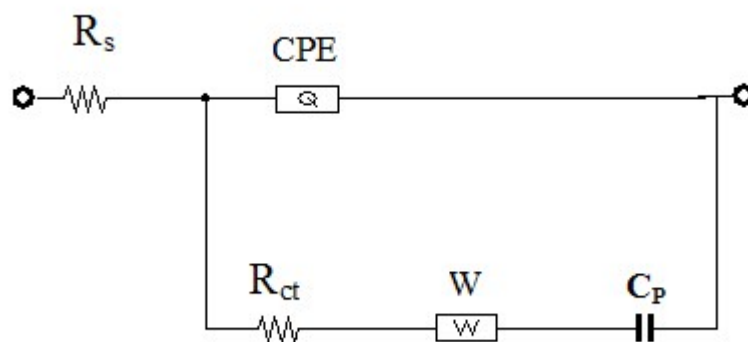
(B)

Figure 11 (A) Electrochemical impedance spectra of the activated carbon vs. EMD (low grade) asymmetric capacitor (a) before and (b) after 2000 cycling in the frequency range from 1 Hz to 100 kHz with AC excitation amplitude of 10 mV, and (B) its equivalent circuit model.

Table 1 XPS Elemental fractions and chemical states of the three EMD materials derived from different precursors

EMD from different precursors	Chemical state / Atom Fraction (%)											
	Wide (survey) spectrum						C (1s)			O (1s)		
	Mn	O	C	N	Cl	Pb	C-C	C-O-C	O-C=O	Mn-O	Mn-OH	Organic O
Low-grade Mn residue	29.8	50.1	16.7	2.7	0.6	-	57.9	28.7	13.5	76.0	22.1	1.9
Mn cake	29.2	49.6	18.0	2.4	0.7	0.1	58.1	27.4	14.5	74.3	23.5	2.2
Synthetic (MnSO$_4$) solution	28.5	49.8	18.4	2.8	0.4	0.1	59.7	26.2	14.2	71.8	25.5	2.7

Table 2 Some manganese dioxide based supercapacitor device in a range of aqueous electrolytes and their energy storage performances.

Electrodes used in a capacitor device	Specific capacitance (F g^{-1})		Energy density (Wh kg^{-1})	Reference
	Cell configuration			
	Two-cell	Three-cell		
Multilayer Fullerenes | 0.5 M H$_2$SO$_4$ | MnO$_2$	N/A	216	30	[29]
Activated Graphene |1M Na$_2$SO$_4$ |Birnessite MnO$_2$	27	N/A	22.5	[30]
Activated Carbon | 0.1M K$_2$SO$_4$| MnO$_2$	21	N/A	10	[37]
Mesoporous Carbon | 0.5 M Na$_2$SO$_4$ | MnO$_2$	N/A	112	15.6	[38]
Graphene oxide | 1M Li$_2$SO$_4$ | EMD-GO composite	77	N/A	10.5	[39]
Activated Carbon | Polymer electrolyte | MnO$_2$	48	N/A	N/A	[40]
Activated Carbon | 2M NaOH | EMD$_{low-grade}$	50	205	17	This work
Graphene oxide | 1M Li$_2$SO$_4$ | GO/α- MnO$_{2(SDS)}$ composite	90	280	35	[39]
Carbon | 1M KOH | rGO-MnO$_2$ composite	N/A	578	70	[41]
Carbon | 1M Na$_2$SO$_4$ | rGO-MnO$_2$ composite	N/A	378	52.5	[42]

Table 3 Equivalent circuit parameters deduced by fitting the impedance plots to the circuit shown in Figure 11B.

EMD (low grade residue)	R$_s$ (Ω) cm^2	R$_{ct}$ (Ω) cm^2	W (Ω) cm^2 s$^{-1/2}$	C$_P$ F cm^{-2}	CPE 10^3 Ω^{-1} cm^{-2} s	n
Before cycling	22.6742	17.3052	1.8	0.42	3.8	0.58
After cycling	40.1894	20.6483	1.3	0.39	1.6	0.55